Imaging the Moho and the Main Himalayan Thrust in Western Nepal With Receiver Functions

Shiba Subedi, György Hetényi, Jerome Vergne, Laurent Bollinger, H Lyon-Caen, Véronique Farra, Lok Bijaya Adhikari, Ratna Mani Gupta

Geophysical Research Letters

RESEARCH LETTER
10.1029/2018GL080911

Key Points:
- Temporary broadband seismic network reveals the crustal structure of Western Nepal using converted waves
- Moho and Main Himalayan Thrust geometry resemble those in Central Nepal, amidst broadscale along-strike variations
- Similarity in crustal configuration means Western Nepal can host M > 8 megathrust events

Supporting Information:
- Supporting Information S1

Correspondence to:
S. Subedi,
shiba.subedi@unil.ch

Citation:
Subedi, S., Hetényi, G., Vergne, J., Bollinger, L., Lyon-Caen, H., Farra, V., et al. (2018). Imaging the Moho and the Main Himalayan Thrust in Western Nepal with receiver functions. *Geophysical Research Letters*, *45*, 13,222–13,230. https://doi.org/10.1029/2018GL080911

Received 17 OCT 2018
Accepted 18 NOV 2018
Accepted article online 21 NOV 2018
Published online 18 DEC 2018

Imaging the Moho and the Main Himalayan Thrust in Western Nepal With Receiver Functions

Shiba Subedi[1,2], György Hetényi[2], Jérôme Vergne[3], Laurent Bollinger[4], Hélène Lyon-Caen[1], Véronique Farra[5], Lok Bijaya Adhikari[6], and Ratna Mani Gupta[7]

[1]Laboratoire de Géologie, Ecole Normale Supérieure/CNRS UMR8538, PSL Research University, Paris, France, [2]Institute of Earth Sciences, University of Lausanne, Lausanne, Switzerland, [3]IPGS-EOST, CNRS/University of Strasbourg, Strasbourg, France, [4]CEA, DAM, DIF, Arpajon, France, [5]Institut de Physique du Globe de Paris, Paris, France, [6]Department of Mines and Geology, National Seismological Centre, Kathmandu, Nepal, [7]Department of Mines and Geology, Regional Seismological Centre, Birendranagar, Nepal

Abstract The crustal structure of Western Nepal is studied for the first time by performing receiver function analysis on teleseismic waveforms recorded at 16 seismic stations. The Moho geometry is imaged as it deepens from ~40-km depth beneath the foothills and the Lesser Himalaya to ~58-km depth beneath the Higher Himalayan range. A midcrustal low-velocity zone is detected at ~15-km depth along ~55-km horizontal distance and is interpreted as the signature of fluids expelled from rocks descending in the footwall of the Main Himalayan Thrust. Our new image allows structural comparison of the Moho and of the Main Himalayan Thrust geometry along-strike of the Himalayas and documents long-wavelength lateral variations. The general crustal architecture observed on our images resembles that of Central Nepal; therefore, Western Nepal is also expected to be able to host large ($M_W > 8$) megathrust earthquakes, as the 1505 CE event.

Plain Language Summary We investigate the Earth's crust in Western Nepal. We use 16 stations to detect waves from far-away earthquakes, and using these we make an image of the structure of the crust. We find that the crust is getting thicker beneath the Himalaya and that fluids are locally present in the upper part of the crust. As this image is similar to the one we know in Central Nepal, where major earthquakes happened, it is possible that major earthquakes will also happen in Western Nepal in the future (without knowing when).

1. Introduction

The Himalayas are the result of the Indian and Eurasian plates' convergence (e.g., Aitchison et al., 2007), which takes place at a rate of ~4 cm/year. About half of this is accommodated by shortening across the Himalayas (e.g., Zheng et al., 2017) on the Main Himalayan Thrust (MHT) fault, the megathrust present under and along the 2,500-km-long Himalayan range. The upper segment of the fault is locked between the surface and its down-dip end, located at a depth of ~20 km under the High Himalayan range (e.g., Bettinelli et al., 2006). This upper, locked segment of the MHT ruptures partially or entirely during large or great earthquakes and thereby propagates the strain accumulated at depth during the interseismic period toward the surface (e.g., Avouac, 2015).

The largest instrumentally recorded earthquake in Nepal, the 1934 M_W8.2 Bihar-Nepal earthquake, has ruptured a >150-km segment of the MHT from Eastern to Central Nepal (Sapkota et al., 2013). It was followed by the Gorkha earthquake (M_W7.8) and a second event (M_W7.3) in 2015 (e.g., Adhikari et al., 2015), which ruptured a consecutive deep segment of the MHT further west in Central Nepal (Avouac et al., 2015; Duputel et al., 2016; Elliott et al., 2016; Grandin et al., 2015; Lindsey et al., 2015). An earthquake in 1833 with macroseismic effects similar to that of the 2015 event was reported in that same region (Bilham, 1995; Martin et al., 2015), it is therefore possible that the 2015 and 1833 earthquakes have ruptured a similar segment of the MHT. However, further west, no large earthquake is documented in the last 500 years (e.g., Hetényi, Le Roux-Mallouf, et al., 2016) since the occurrence of the major 1505 CE earthquake (Ambraseys & Jackson, 2003), leading to a well-identified seismic gap (e.g., Bollinger et al., 2016; Khattri, 1987; Kumar et al., 2006; Mugnier et al., 2013; Rajendran et al., 2015). The Global Positioning System velocity field measured through this segment of the orogen demonstrates that the upper portion of the MHT is locked (e.g., Stevens & Avouac,

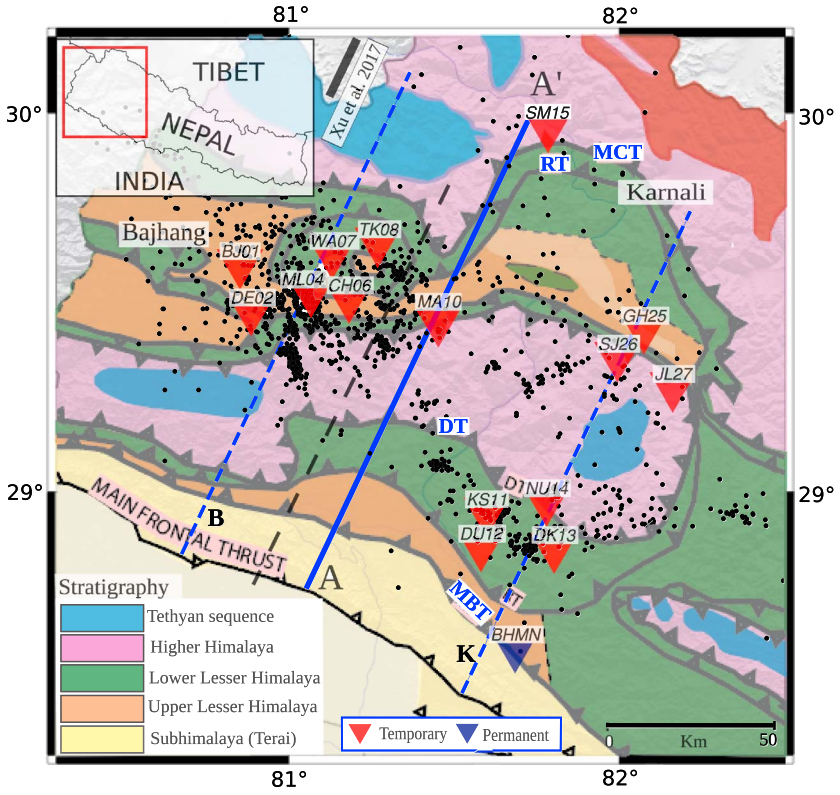

Figure 1. Study area in Western Nepal with the simplified geological map from Robinson et al. (2006). South of the Main Frontal Thrust are foreland basin sediments. Seismic stations operated under Hi-KNet are shown as red triangles and detected seismicity in black dots (Hoste-Colomer et al., 2018). Blue triangle represents a permanent broadband station. Faults: Main Frontal Thrust (MFT), Main Boundary Thrust (MBT), Ramgarh Thrust (RT), Dadeldhura Thrust (DT), Main Central Thrust (MCT). Cross section AA′ is shown on Figures 2 and 3. The thick black line locates the southern end of Xu et al. (2017) profile (Figure 3). Black dashed line locates the Chainpur geological cross section (Robinson & McQuarrie, 2012). Blue dashed lines B and K locate the Bajhang and Karnali profiles (Figures S5 and S6). Inset locates the map within Nepal.

2016) and may have accumulated as much as ~10 m of slip deficit. Given the estimate of average earthquake return period along the Himalayas (Avouac et al., 2001; Bollinger et al., 2014; Stevens & Avouac, 2016), the area of the 1505 CE earthquake is highly prone for a major ($M_W > 8$) megathrust event.

Since the structure of the crust and the geometry of the MHT are key parameters to better understand seismogenesis and to evaluate seismic hazard, several temporary seismic experiments were deployed to image the crustal structure in Nepal. The experiment Himalayan Nepal Tibet Seismic Experiment imaged the structures across a 300-km-long and 300-km-wide network (Schulte-Pelkum et al., 2005) in East Nepal and southern Tibet. The Hi-CLIMB experiment has carried out high-resolution imaging of structures along an 800-km-long profile across Central Nepal (Hetényi, 2007; Nábělek et al., 2009) and central Tibet. This data set allowed Duputel et al. (2016) to associate the rupture of the 2015 Gorkha earthquake along the flat portion of the MHT with a low-velocity zone (LVZ) constrained by both CMT inversion and P-seismic and S-seismic receiver function (RF) approach. However, in Western Nepal, there is currently no geophysical image of crustal structures available. The MHT geometry remains therefore elusive, leaving the question of the applicability of the Central Nepal seismogenic model in the area of the great 1505 CE earthquake open.

Indeed, the surface geology of the fold-and-thrust belt in Western Nepal is significantly different from Central Nepal. It exposes a more complex stack of alternating Lesser Himalayan slivers and crystalline klippe relicts (Figure 1; Arita et al., 1984; DeCelles et al., 2001; Robinson et al., 2006; Robinson & McQuarrie, 2012). The geometry of the fold-and-thrust belt allowed reconstituting balanced cross sections of the area (Robinson et al., 2006; Robinson & McQuarrie, 2012) that were never confronted with geophysical constraints apart from the regional seismological catalogue (Pandey et al., 1999). This catalogue depicts lateral variations of the seismicity but their hypocentral depths were not well constrained.

A temporary seismic network was recently deployed in Western Nepal to scrutinize regional seismic activity (Hoste-Colomer et al., 2018; Figure 1). In this article, we analyze the data recorded by the same network to image the crustal structure of Western Nepal for the first time. We chose to work with the RF method (e.g., Langston, 1977), which is best suited to map lithospheric discontinuities with sharp velocity changes. This way we primarily aim at the crust-mantle boundary (Moho) and at potential LVZs in the crust, as observed in Central Nepal. We compare our results to other cross sections across the Himalaya and especially to Central Nepal for structural and seismogenetic aspects.

2. Data and Methods

2.1. Data

This study is based on data recorded at 15 stations of the first temporary seismic experiment in Western Nepal, the Himalaya-Karnali-Network (Hi-KNet) and permanent station BHMN (see supporting information Text S1). All stations used three-component, broadband, or intermediate-period sensors (see Table S1). The network geometry was defined to best analyze local seismicity by covering the different earthquake belts in Western Nepal, thus forming three clusters of stations (Figure 1) with an average station spacing of ~10 km in each.

For the computation of RFs, we selected $M_W \geq 5.5$ teleseismic earthquakes at epicentral distances 30–100° from the U.S. Geological Survey earthquake catalogue (Figure S1). The Hi-KNet recorded 372 such earthquakes during its operation, and station BHMN recorded 160 such events between March 2014 and September 2015.

2.2. RF Computation

The original ZNE-component data are band-pass filtered between 0.2 and 0.5 Hz for single station analysis and 0.2 and 1 Hz for RF migration (section 2.3). Semiautomatic quality-control criteria were adopted following Hetényi et al. (2015, 2018) and Singer et al. (2017; see supporting information Text S1). Seismograms were rotated into the ray-based *LQT* (P-S_V-S_H) coordinate system using the theoretical ray parameter and assumed near-surface velocity (see model description below). This way the direct P phase is removed during deconvolution, therefore no or little signal should appear at zero lag time. The *Q* and *T* components were then deconvolved from the *L* component using the time-domain iterative approach of Ligorría and Ammon (1999) using 150 iterations, and the spikes convolved with a Gaussian pulse of a width corresponding to the signal's highest frequency to obtain the final radial and transverse RFs. A visual quality control on RFs discarded few poor quality and anomalous RFs (e.g., ringing waveforms, no clear Ps phase). Our final data set consists of 960 high-quality RFs, shown in Figure S2 (radial and transverse components) and Figure S3 in cross section view of station-stacked radial RFs along the AA′ profile.

2.3. RF Analysis

In frame of our RF analysis we employ two methods, detailed below. First, a single-station approach to validate that the first-order structure of the crust resembles that of the local velocity model chosen for migration in terms of average crustal V_p/V_s. Then, to construct our final images using a more sophisticated approach, we perform prestack time-to-depth migration and interpret the results based on those.

For the first step, we follow the H-K approach (Zhu & Kanamori, 2000) where the time separation between the direct P phase, the converted Ps phase and the multiply reverberated phases are exploited (Figure S4). We consider the extent of the H-K-space peak (at a nominal 86% of the maximum amplitude) to estimate the related uncertainties of both values (Table S2 and Figure S4). The main goal of this single-station analysis is to see how the derived V_p/V_s ratios compare with the previously proposed 1-D velocity model and whether this model can be reasonably used for RF migration. Our results demonstrate that the average crustal V_p/V_s for all except one station (BHMN) justifies the use of a 1-D velocity model in the migration approach.

To draw final interpretations we perform time-to-depth migration and spatially reconstruct the geometries of the subsurface discontinuities causing the wave conversions. We use the widely adopted common conversion point migration technique (e.g., Zhu, 2000) (see parameters in supporting information Text S1). We chose the Nepali national velocity model (Pandey et al., 1995) for the ray tracing and time-to-depth conversion, as this is the only available well-constrained model in the broader region (Table S3). At the only

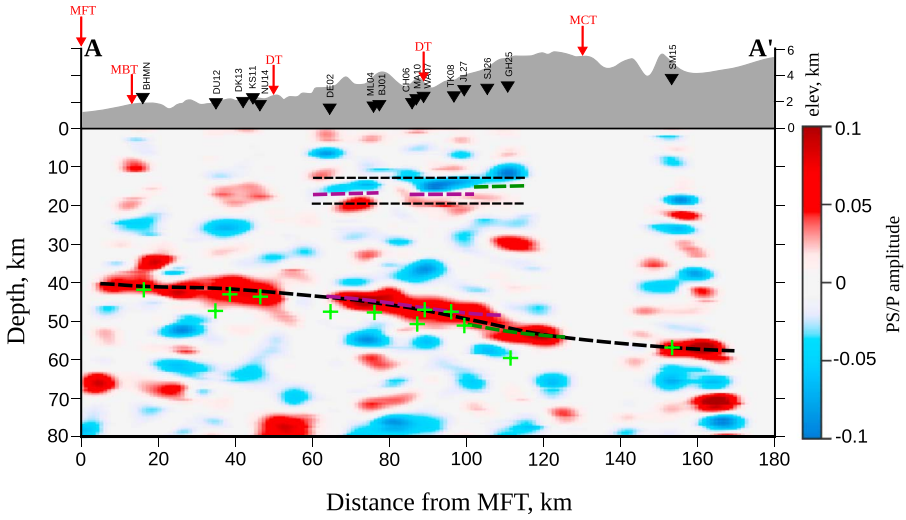

Figure 2. P-to-S receiver function migration imaging the crust. The prominent signal from the Moho and the intracrustal low-velocity zone are highlighted with black dashed line drawing. Green crosses show Moho depths computed from H-K stacking. Dashed purple and green lines are reported from Bajhang and Karnali profiles, respectively (Figures S5 and S6), where local lateral variation of Moho depth and/or velocities is hypothesized. Fault name abbreviations as in Figure 1. See text for detailed discussion. MFT = Main Frontal Thrust; MBT = Main Boundary Thrust; DT = Dadeldhura Thrust; MCT = Main Central Thrust.

station where the average crustal V_p/V_s estimate (BHMN: 1.60) differs from that of the Nepali velocity model (1.75–1.76), we modify the V_s model used in the migration: we create a 1-D model by dividing the Nepali model's V_p by the station's average crustal V_p/V_s obtained from H-K stacking. Other stations do not require correction as they detect V_p/V_s values (1.69–1.81) that are similar to that of the Nepali velocity model (1.75–1.76). This is corroborated by the V_p/V_s range of 1.75 ± 0.06 obtained from Wadati diagrams generated with 67 events beneath northern Hi-KNet during the experiment (Benoit, 2016). We assess the uncertainty of our Moho depth determinations and conclude that our results are consistent and robust (see supporting information Text S1).

Migration results are presented along the AA′ profile (Figure 2) and separately for the Bajhang and Karnali profiles (Figures S5 and S6). To extend our main RF profile and the interpretation, we append the migrated RF image of Xu et al. (2017) in southern Tibet (Figure 3), continuing in the same direction and offset by 75 km to the west, properly juxtaposed to our image.

3. Results

The migrated RF images reveal for the first time the crustal structure of Western Nepal (Figure 2). The consistent, positive (velocity increase with depth) interface is interpreted as the Moho. Despite the lateral spread of stations, the Moho signature is sharp and clear. The observed Moho depth beneath BHMN station is ~40 km, and it slowly increases toward the north, reaching ~58 km beneath the Higher Himalaya. The imaged shape of the Moho is smooth along the AA′ profile except at ~110-km distance where different Moho depths are projected near each other from the Bajhang and Karnali profiles (Figures S5 and S6). The maximum Moho depth difference there is ~6 km and hints at local lateral variations over the ~100-km distance between the two profiles. This difference could arise from locally varying velocities along the arc, not accounted for by the employed 1-D velocity model. Our results are stable across different frequency bands between 0.2 and 2 Hz.

Besides the Moho the strongest and most continuous signal observed in the crust is a negative-over-positive (blue-over-red) amplitude feature in the central part of the profile. It is present both along the Bajhang and Karnali profiles (Figures S5 and S6). The apparent interruption at ~80-km distance can be due to shallow, local variations in structure or velocity with respect to the model used during migration.

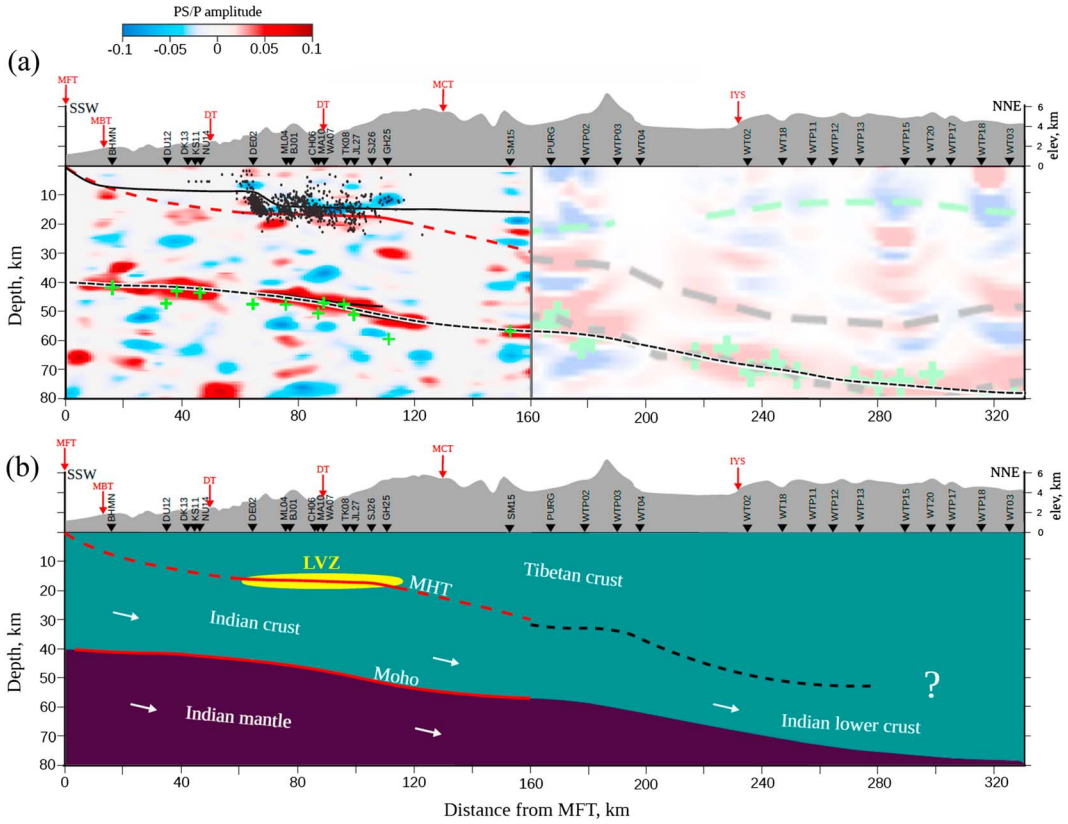

Figure 3. Extended profile and interpretation. (a) Composite receiver function image from Figure 2 (left) and from Xu et al. (2017; right, reduced color intensity). Green crosses: Moho depths derived by H-K stacking in this study. Black dashed line: smoothed, interpreted Moho from common conversion point migration. Red line: position of the MHT at the central depth of the LVZ; dashed parts are extrapolations. Thick black line: MHT geometry interpreted from geological reconstructions (Robinson & McQuarrie, 2012). Black dots: locally detected seismicity by Hi-KNet (Hoste-Colomer et al., 2018). Note that the Xu et al. (2017) profile is offset by ~75 km to the west and has been processed differently than our profile, but we juxtaposed it properly to our image using their station-wise Moho depth estimates (green crosses based on differential delay times of Ps and PpPs Moho phases from station-stacked P receiver functions). Their thick black dashed lines: interpretation of the Moho and an intracrustal discontinuity. Their green dashed line: top of another type of LVZ that are characteristic of southern Tibet and not discussed here. (b) Interpretive sketch showing the configuration of the underthrusting Indian plate beneath the Himalayas and the Tibetan plateau. Our observations of the Moho and MHT are represented in red solid lines, and the extrapolations of the MHT in red dashed lines. Dashed black line on the right side indicates the intracrustal discontinuity as drawn by Xu et al. (2017). White arrows represent motion of the India plate relative to Tibet. Fault name abbreviations as in Figure 1. DT = Dadeldhura Thrust; LVZ = low-velocity zone; MBT = Main Boundary Thrust; MCT = Main Central Thrust; MFT = Main Frontal Thrust; MHT = Main Himalayan Thrust; IYS = Indus–Yarlung Suture.

This seismic signature corresponds to a velocity decrease at ~12- to 14-km depth followed by a velocity increase at ~18-km depth, indicating the presence of a subhorizontal, ~55-km-long LVZ. It expands between ~60- and ~115-km distance north of the Main Frontal Thrust, beneath a region of imbricated thrust sheets (Hoste-Colomer et al., 2018; Robinson & McQuarrie, 2012) of Lesser Himalayan rocks called the main Lesser Himalayan duplex (Figures 1 and 2). Due to the absence of major velocity discontinuities at shallower depth, it is unlikely that this signal corresponds to multiple reverberations. There can also be some local effects of dip and/or anisotropy, as some stations feature high amplitudes on the transverse RFs. However, we cannot conclude on these aspects due to incomplete back-azimuthal coverage (Figure S2). In the absence of reliable information on dip and anisotropy and of coherent transverse signal across our array, we assume that the negative-over-positive features are caused by the top and the bottom of an LVZ. Furthermore, the fact that this LVZ is observed on both profiles (Figures S5 and S6) and also elsewhere in the Himalaya (see below) corroborates our interpretation and indicates that the LVZ is pervasive along-strike of the orogen.

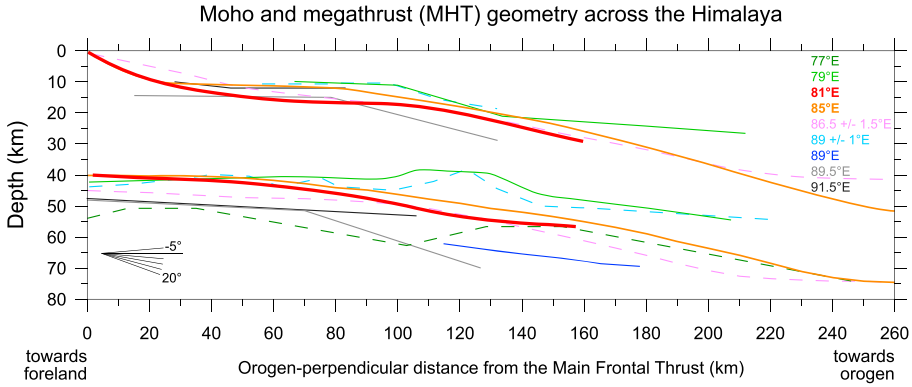

Figure 4. Along-strike comparison of Moho and MHT geometry across the Himalayan orogen. The information are taken from profiles at 77°E (Rai et al., 2006), 79°E (Caldwell et al., 2013), 81°E (this study), 85°E (Hetényi, 2007), 86.5 ± 1.5°E (Schulte-Pelkum et al., 2005), 89 ± 1°E (Acton et al., 2011), 89°E (Hauck et al., 1998), 89.5°E, and 91.5°E (Singer et al., 2017). The drawing of the 77°E, the 79°E, and the 89 ± 1°E profiles are adapted from Caldwell et al.'s (2013) figure. To account for proper projection, all other profiles are freshly redrawn to scale. Profiles with sparse data or wider lateral smoothing are shown in dashed lines. All these results stem from receiver function analysis, except for the 89°E profile, which is from active seismics. MHT = Main Himalayan Thrust.

4. Interpretation and Discussion

Our interpretation is based on the most robust results revealed by RF imaging (Figures 2 and 3). The Moho geometry connects well with the one derived from *P* wave RFs in southern Tibet (Xu et al., 2017), with discrepancies of less than 5 km at their southernmost stations, reasonable for lateral variation over the ~75-km distance separating the two profiles.

In Western Nepal, the distance over which the Moho reaches its maximum depth differs from Central Nepal (Figure 4; Nábělek et al., 2009): The gentler descent ends further north, north of the Higher Himalaya, at nearly 80-km depth beneath southern Tibet (Xu et al., 2017). This may reflect a slightly different flexural rigidity of the India plate in Western Nepal compared to Central Nepal, although there is no significant difference in flexure West and East of our profile in Nepal as seen by gravity anomalies and numerical modeling (Berthet et al., 2013), unlike further toward NW India and to the Eastern Himalaya (Hammer et al., 2013; Hetényi, Cattin, et al., 2016; Lyon-Caen & Molnar, 1985).

The general appearance and northward deepening shape of the Moho in Western Nepal is similar to the geometry in Central Nepal at longitude 85°E (Nábělek et al., 2009; Figure 4). However, Moho depth variations exceeding 10 km and variation in the flexural descent position vary significantly when compared to numerous other profiles across the orogen (Figure 4). Although some of these differences stem from variable processing of seismological data (mostly common conversion point migration of RFs but with different velocity models) in different studies and uneven data coverage, the shown variability can contain true structural elements that reflect inherited structure of the India plate entering the collision zone (Hetényi, Cattin, et al., 2016).

The LVZ identified from clear negative-over-positive amplitudes (Figures 2 and 3) along a ~55-km-long segment is similar to the one observed in Central Nepal (Duputel et al., 2016; Nábělek et al., 2009) although we observe it ~15 km further north, more distant from the Main Frontal Thrust. Our imaged LVZ agrees with similar features beneath the Satluj valley, northwest Himalaya (Hazarika et al., 2017). We interpret this feature as a seismic LVZ, due to the local accumulation of fluids originating from metamorphic dehydration reactions of the sediments underthrusted beneath the MHT. Indeed, the analysis of fluid inclusions of quartz exudates sampled within the MCT shear zone—which is a remnant of the MHT—demonstrates that both aqueous fluids (mainly brines) and CO_2-bearing inclusions, from metamorphic and meteoric origins, were injected from midcrustal to shallower depths (e.g., Pecher, 1979). This result is consistent with the thermokinematic evolution of the Himalayan range (e.g., Bollinger et al., 2006). This geological observation is corroborated by the position in Central Nepal of a low-resistivity anomaly at midcrustal depths, deciphered by magneto-telluric sounding, which also inferred the presence of fluids along the MHT's flat portion (Lemonnier et al.,

1999). In Central Nepal, this same LVZ highlights position of the MHT along which rupture propagated during the 2015 Gorkha earthquake (Duputel et al., 2016). In NW India, beneath the Garhwal Himalaya, a similar interpretation is made by Caldwell et al. (2013). Therefore, we interpret the LVZ in Western Nepal as the position of the MHT and draw the MHT at the central depth of the LVZ as Duputel et al. (2016) and other, earlier studies.

We also compare our results with the Chainpur and Simikot geological cross sections from Robinson et al. (2006): The seismically imaged LVZ fits very well the position of geological MHT within uncertainties inherent to the methods. The depth of the LVZ's top corresponds to the depth of the lower décollement deduced from balanced cross sections (Figure 3a), while our interpretation for the MHT (central depth of the LVZ) is ~3 km deeper. A locally steep ramp as the one at ~65-km distance proposed from the geological cross section could produce some of the transverse RF signal (Figure S2), but better station and back-azimuthal coverage would be needed to constrain it. Finally, this LVZ is matching perfectly the midcrustal seismic cluster recently characterized in Western Nepal by our temporary network (Hoste-Colomer et al., 2018; Figure 3), which suggests that the depth range around the megathrust is critically stressed.

Our images reveal a similar character but somewhat different depth of the MHT and of the Moho in Western Nepal compared to Central Nepal. On the scale of the orogen, long-wavelength along-strike variations are clearly present (Figure 4). The transition between the mapped geometries along profiles could materialize in lateral ramps, also pointed to by seismicity studies in our study area (Hoste-Colomer et al., 2018), which may segment seismic ruptures laterally. Despite these variations, the overall similarity of the crustal geometries between Western and Central Nepal highlights a smoothly northward dipping flexural shape. This suggests that the boundary conditions to seismogenesis in Western Nepal are broadly the same as in Central Nepal. Therefore, the expected rupture characteristics and scenarios are also similar, suggesting that we can expect large ($M_W > 8$) megathrust earthquakes in Western Nepal in the area where there has not been a major event since 1505 CE.

5. Conclusions

This study, using data recorded by a 2-year, temporary broadband seismological network in Western Nepal and analyzed with the RF approach, allows us to conclude the following:

1. The Moho in Western Nepal is gently dipping northward, from a depth of ~40 km beneath the foothills to ~58 km beneath the Higher Himalaya and then further beneath southern Tibet.
2. A midcrustal LVZ is observed along ~55-km distance, at ~12- to 18-km depth, beneath the Lesser Himalaya. This LVZ is likely caused by fluids expelled from the underthrusting sedimentary rocks and trapped at the Main Himalayan Thrust. Our geophysical image is consistent with the depth of the MHT revealed by a geologically balanced cross section and a midcrustal seismic cluster.
3. The crustal structure of Western Nepal is broadly similar to that of Central Nepal, but lateral variations exist further away along the mountain belt. These may be connected by lateral ramps, which may influence or segment seismic ruptures along-strike of the orogen.
4. The crustal configuration of Western Nepal is broadly similar to that in Central Nepal and the Garhwal Himalaya. Therefore, the processes of major earthquake generation should be alike, favoring scenarios of a megathrust event in the Western Nepal seismic gap that has not ruptured since 1505 CE.

Acknowledgments
The seismological instruments deployed in Western Nepal in project Hi-KNet (https://doi.org/10.15778/RESIF.ZO2014) belong to the French pool of portable seismic instruments Sismob-RESIF. We sincerely thank Roser Hoste-Colomer and the Hi-KNet team for data collection. We are grateful to the Nepalese Department of Mines and Geology for providing BHMN data and for supporting the installation of Hi-KNet. The Hi-KNet seismological data will be made available at http://seismology.resif.fr in 01.2020. The temporary network project was funded through the French ANR (project BHUTANEPAL, grant 13-BS06-0006-01). The research was partly financed by CEA/DASE and hosted at the Yves Rocard Joint Laboratory (ENS-CNRS-CEA/DASE). The contribution of the Swiss National Science Foundation (grant PP00P2_157627, project OROG3NY) is acknowledged. S. Subedi thanks Y. Klinger and IPGP for hosting him during his research internship. We greatly thank the constructive suggestions from anonymous reviewers that very much helped improve this manuscript.

References

Acton, C. E., Priestley, K., Mitra, S., & Gaur, V. K. (2011). Crustal structure of the Darjeeling-Sikkim Himalaya and southern Tibet. *Geophysical Journal International*, *184*(2), 829–852. https://doi.org/10.1111/j.1365-246X.2010.04868.x

Adhikari, L. B., Gautam, U. P., Koirala, B. P., Bhattarai, M., Kandel, T., Gupta, R. M., et al. (2015). The aftershock sequence of the 2015 April 25 Gorkha-Nepal earthquake. *Geophysical Supplements to the Monthly Notices of the Royal Astronomical Society*, *203*(3), 2119–2124. https://doi.org/10.1093/gji/ggv412

Aitchison, J. C., Ali, J. R., & Davis, A. M. (2007). When and where did India and Asia collide? *Journal of Geophysical Research*, *112*, B05423. https://doi.org/10.1029/2006JB004706

Ambraseys, N., & Jackson, D. (2003). A note on early earthquakes in northern India and southern Tibet. *Current Science*, *84*, 570–582.

Arita, K., Shiraishi, K., & Hayashi, D. (1984). Geology of Western Nepal and a comparison with Kumaun, India. *Journal of the Faculty of Science, Hokkaido University, series 4, Geology and mineralogy*, *21*(1), 1–20.

Avouac, J. P. (2015). *Mountain building: From earthquakes to geologic deformation*. Cambridge, UK: University of Cambridge.

Avouac, J. P., Bollinger, L., Lavé, J., Cattin, R., & Flouzat, M. (2001). Le cycle sismique en Himalaya. *Comptes Rendus de l'Académie des Sciences-Series IIA-Earth and Planetary Science*, *333*(9), 513–529.

Avouac, J. P., Meng, L., Wei, S., Wang, T., & Ampuero, J. P. (2015). Lower edge of locked Main Himalayan Thrust unzipped by the 2015 Gorkha earthquake. *Nature Geoscience*, *8*(9), 708–711. https://doi.org/10.1038/ngeo2518

Benoit, A. (2016). Apport de la microsismicité dans l'étude des grands chevauchements himalayens, (MSc thesis, pp. 1–30). University Montpellier.

Berthet, T., Hetényi, G., Cattin, R., Sapkota, S. N., Champollion, C., Kandel, T., et al. (2013). Lateral uniformity of India Plate strength over central and eastern Nepal. *Geophysical Journal International*, *195*(3), 1481–1493. https://doi.org/10.1093/gji/ggt357

Bettinelli, P., Avouac, J. P., Flouzat, M., Jouanne, F., Bollinger, L., Willis, P., & Chitrakar, G. R. (2006). Plate motion of India and interseismic strain in the Nepal Himalaya from GPS and DORIS measurements. *Journal of Geodesy*, *80*(8–11), 567–589. https://doi.org/10.1007/s00190-006-0030-3

Bilham, R. (1995). Location and magnitude of the 1833 Nepal earthquake and its relation to the rupture zones of contiguous great Himalayan earthquakes. *Current Science*, *69*(2), 101–128.

Bollinger, L., Henry, P., & Avouac, J. P. (2006). Mountain building in the Nepal Himalaya: Thermal and kinematic model. *Earth and Planetary Science Letters*, *244*(1–2), 58–71. https://doi.org/10.1016/j.epsl.2006.01.045

Bollinger, L., Sapkota, S. N., Tapponnier, P., Klinger, Y., Rizza, M., Van der Woerd, J., et al. (2014). Estimating the return times of great Himalayan earthquakes in eastern Nepal: Evidence from the Patu and Bardibas strands of the Main Frontal Thrust. *Journal of Geophysical Research: Solid Earth*, *119*, 7123–7163. https://doi.org/10.1002/2014JB010970

Bollinger, L., Tapponnier, P., Sapkota, S. N., & Klinger, Y. (2016). Slip deficit in Central Nepal: Omen for a repeat of the 1344AD earthquake? *Earth, Planets and Space*, *68*(1), 1–12. https://doi.org/10.1186/s40623-016-0389-1

Caldwell, W. B., Klemperer, S. L., Lawrence, J. F., & Rai, S. S. (2013). Characterizing the Main Himalayan Thrust in the Garhwal Himalaya, India with receiver function CCP stacking. *Earth and Planetary Science Letters*, *367*, 15–27. https://doi.org/10.1016/j.epsl.2013.02.009

DeCelles, P. G., Robinson, D. M., Quade, J., Ojha, T. P., Garzione, C. N., Copeland, P., & Upreti, B. N. (2001). Stratigraphy, structure, and tectonic evolution of the Himalayan fold-thrust belt in Western Nepal. *Tectonics*, *20*(4), 487–509. https://doi.org/10.1029/2000TC001226

Duputel, Z., Vergne, J., Rivera, L., Wittlinger, G., Farra, V., & Hetényi, G. (2016). The 2015 Gorkha earthquake: A large event illuminating the Main Himalayan Thrust fault. *Geophysical Research Letters*, *43*, 2517–2525. https://doi.org/10.1002/2016GL068083

Elliott, J. R., Jolivet, R., González, P. J., Avouac, J. P., Hollingsworth, J., Searle, M. P., & Stevens, V. L. (2016). Himalayan megathrust geometry and relation to topography revealed by the Gorkha earthquake. *Nature Geoscience*, *9*(2), 174–180. https://doi.org/10.1038/ngeo2623

Grandin, R., Vallée, M., Satriano, C., Lacassin, R., Klinger, Y., Simoes, M., & Bollinger, L. (2015). Rupture process of the Mw = 7.9 2015 Gorkha earthquake (Nepal): Insights into Himalayan megathrust segmentation. *Geophysical Research Letters*, *42*, 8373–8382. https://doi.org/10.1002/2015GL066044

Hammer, P., Berthet, T., Hetényi, G., Cattin, R., Drukpa, D., Chophel, J., et al. (2013). Flexure of the India plate underneath the Bhutan Himalaya. *Geophysical Research Letters*, *40*, 4225–4230. https://doi.org/10.1002/grl.50793

Hauck, M. L., Nelson, K. D., Brown, L. D., Zhao, W., & Ross, A. R. (1998). Crustal structure of the Himalayan orogen at ~90° east longitude from Project INDEPTH deep reflection profiles. *Tectonics*, *17*(4), 481–500. https://doi.org/10.1029/98TC01314

Hazarika, D., Wadhawan, M., Paul, A., Kumar, N., & Borah, K. (2017). Geometry of the Main Himalayan Thrust and Moho beneath Satluj valley, northwest Himalaya: Constraints from receiver function analysis. *Journal of Geophysical Research: Solid Earth*, *122*, 2929–2945. https://doi.org/10.1002/2016JB013783

Hetényi, G. (2007). Evolution of deformation of the Himalayan prism: From imaging to modelling, (PhD thesis, 400 pp.). École Normale Supérieure-Université Paris-Sud XI. Retrieved from http://tel.archives-ouvertes.fr/tel-00194619/en/

Hetényi, G., Cattin, R., Berthet, T., Le Moigne, N., Chophel, J., Lechmann, S., et al. (2016). Segmentation of the Himalayas as revealed by arc-parallel gravity anomalies. *Scientific Reports*, *6*(1), 33866. https://doi.org/10.1038/srep33866

Hetényi, G., Le Roux-Mallouf, R., Berthet, T., Cattin, R., Cauzzi, C., Phuntsho, K., & Grolimund, R. (2016). Joint approach combining damage and paleoseismology observations constrains the 1714 A.D. Bhutan earthquake at magnitude 8±0.5. *Geophysical Research Letters*, *43*, 10,695–10,702. https://doi.org/10.1002/2016GL071033

Hetényi, G., Plomerová, J., Bianchi, I., Kampfová Exnerová, H., Bokelmann, G., Handy, M. R., Babuška, V., & AlpArray-EASI Working Group (2018). From mountain summits to roots: Crustal structure of the Eastern Alps and Bohemian Massif along longitude 13.3°E. *Tectonophysics*. https://doi.org/10.1016/j.tecto.2018.07.001

Hetényi, G., Ren, Y., Dando, B., Stuart, G. W., Hegedűs, E., Kovács, A. C., & Houseman, G. A. (2015). Crustal structure of the Pannonian Basin: The AlCaPa and Tisza terrains and the mid-Hungarian zone. *Tectonophysics*, *646*, 106–116. https://doi.org/10.1016/j.tecto.2015.02.004

Hoste-Colomer, R., Bollinger, L., Lyon-Caen, H., Adhikari, L. B., Baillard, C., Benoit, A., et al. (2018). Lateral variations of the midcrustal seismicity in western Nepal: Seismotectonic implications. *Earth and Planetary Science Letters*, *504*, 115–125. https://doi.org/10.1016/j.epsl.2018.09.041

Khattri, K. N. (1987). Great earthquakes, seismicity gaps and potential for earthquake disaster along the Himalaya plate boundary. *Tectonophysics*, *138*(1), 79–92. https://doi.org/10.1016/0040-1951(87)90067-9

Kumar, S., Wesnousky, S. G., Rockwell, T. K., Briggs, R. W., Thakur, V. C., & Jayangondaperumal, R. (2006). Paleoseismic evidence of great surface-rupture earthquakes along the Indian Himalaya. *Journal of Geophysical Research*, *111*, B03304. https://doi.org/10.1029/2004JB003309

Langston, C. (1977). Corvallis, Oregon, crustal and upper mantle receiver structure from teleseismic P-waves and S-waves. *Bulletin of the Seismological Society of America*, *67*(3), 713–724.

Lemonnier, C., Marquis, G., Perrier, F., Avouac, J. P., Chitrakar, G., Kafle, B., et al. (1999). Electrical structure of the Himalaya of Central Nepal: High conductivity around the mid-crustal ramp along the MHT. *Geophysical Research Letters*, *26*(21), 3261–3264. https://doi.org/10.1029/1999GL008363

Ligorría, J. P., & Ammon, C. J. (1999). Iterative deconvolution and receiver-function estimation. *Bulletin of the Seismological Society of America*, *89*(5), 1395–1400.

Lindsey, E. O., Natsuaki, R., Xu, X., Shimada, M., Hashimoto, M., Melgar, D., & Sandwell, D. T. (2015). Line-of-sight displacement from ALOS-2 interferometry: Mw 7.8 Gorkha Earthquake and Mw 7.3 aftershock. *Geophysical Research Letters*, *42*, 6655–6661. https://doi.org/10.1002/2015GL065385

Lyon-Caen, H., & Molnar, P. (1985). Gravity anomalies, flexure of the India Plate, and the structure, support and evolution of the Himalaya and Ganga Basin. *Tectonics*, *4*(6), 513–538. https://doi.org/10.1029/TC004i006p00513

Martin, S. S., Hough, S. E., & Hung, C. (2015). Ground motions from the 2015 Mw 7.8 Gorkha, Nepal, earthquake constrained by a detailed assessment of macroseismic data. *Seismological Research Letters*, *86*(6), 1524–1532. https://doi.org/10.1785/0220150138

Mugnier, J. L., Gajurel, A., Huyghe, P., Jayangondaperumal, R., Jouanne, F., & Upreti, B. (2013). Structural interpretation of the great earthquakes of the last millennium in the central Himalaya. *Earth-Science Reviews*, *127*, 30–47. https://doi.org/10.1016/j.earscirev.2013.09.003

Nábělek, J., Hetényi, G., Vergne, J., Sapkota, S., Kafle, B., Jiang, M., et al. (2009). Underplating in the Himalaya-Tibet collision zone revealed by the Hi-CLIMB experiment. *Science*, *325*(5946), 1371–1374. https://doi.org/10.1126/science.1167719

Pandey, M. R., Tandukar, R. P., Avouac, J. P., Lave, J., & Massot, J. P. (1995). Interseismic strain accumulation on the Himalayan crustal ramp (Nepal). *Geophysical Research Letters*, *22*(7), 751–754. https://doi.org/10.1029/94GL02971

Pandey, M. R., Tandukar, R. P., Avouac, J. P., Vergne, J., & Heritier, T. (1999). Seismotectonics of the Nepal Himalaya from a local seismic network. *Journal of Asian Earth Sciences*, *22*(7), 751–754. https://doi.org/10.1029/94GL02971

Pecher, A. (1979). Les inclusions fluides des quartz d'exsudation de la zone du MCT himalayen au Népal central: données sur la phase fluide dans une grande zone de cisaillement crustal. *Bulletin de Mineralogie*, *102*, 537–554.

Rai, S. S., Priestley, K., Gaur, V. K., Mitra, S., Singh, M. P., & Searle, M. (2006). Configuration of the Indian Moho beneath the NW Himalaya and Ladakh. *Geophysical Research Letters*, *33*, L15308. https://doi.org/10.1029/2006GL026076

Rajendran, C. P., John, B., & Rajendran, K. (2015). Medieval pulse of great earthquakes in the central Himalaya: Viewing past activities on the frontal thrust. *Journal of Geophysical Research: Solid Earth*, *120*, 1623–1641. https://doi.org/10.1002/2014JB011015

Robinson, D. M., DeCelles, P. G., & Copeland, P. (2006). Tectonic evolution of the Himalayan thrust belt in Western Nepal: Implications for channel flow models. *Geological Society of America Bulletin*, *118*(7–8), 865–885. https://doi.org/10.1130/B25911.1

Robinson, D. M., & McQuarrie, N. (2012). Pulsed deformation and variable slip rates within the central Himalayan thrust belt. *Lithosphere*, *4*(5), 449–464. https://doi.org/10.1130/L204.1

Sapkota, S. N., Bollinger, L., Klinger, Y., Tapponnier, P., Gaudemer, Y., & Tiwari, D. (2013). Primary surface ruptures of the great Himalayan earthquakes in 1934 and 1255. *Nature Geoscience*, *6*(1), 71–76. https://doi.org/10.1038/ngeo1669

Schulte-Pelkum, V., Monsalve, G., Sheehan, A., Pandey, M. R., Sapkota, S., Bilham, R., & Wu, F. (2005). Imaging the Indian subcontinent beneath the Himalaya. *Nature*, *435*(7046), 1222–1225. https://doi.org/10.1038/nature03678

Singer, J., Kissling, E., Diehl, T., & Hetényi, G. (2017). The underthrusting Indian crust and its role in collision dynamics of the Eastern Himalaya in Bhutan: Insights from receiver function imaging. *Journal of Geophysical Research: Solid Earth*, *122*, 1152–1178. https://doi.org/10.1002/2016JB013337

Stevens, V. L., & Avouac, J.-P. (2016). Millenary Mw $>$ 9.0 earthquakes required by geodetic strain in the Himalaya. *Geophysical Research Letters*, *43*, 1118–1123. https://doi.org/10.1002/2015GL067336

Xu, Q., Zhao, J., Yuan, X., Liu, H., & Pei, S. (2017). Detailed configuration of the underthrusting Indian lithosphere beneath western Tibet revealed by receiver function images. *Journal of Geophysical Research: Solid Earth*, *122*, 8257–8269. https://doi.org/10.1002/2017JB014490

Zheng, G., Wang, H., Wright, T. J., Lou, Y., Zhang, R., Zhang, W., et al. (2017). Crustal deformation in the India-Eurasia collision zone from 25 years of GPS measurements. *Journal of Geophysical Research: Solid Earth*, *122*, 9290–9312.

Zhu, L. (2000). Crustal structure across the San Andreas Fault, southern California from teleseismic converted waves. *Earth and Planetary Science Letters*, *179*(1), 183–190. https://doi.org/10.1016/S0012-821X(00)00101-1

Zhu, L., & Kanamori, H. (2000). Moho depth variation in southern California from teleseismic receiver functions. *Journal of Geophysical Research*, *105*(B2), 2969–2980. https://doi.org/10.1029/1999JB900322